Flux-Dependent Growth Kinetics and Diameter Selectivity in Single-Wall Carbon Nanotube Arrays

David B. Geohegan,[†,*] Alex A. Puretzky,[†] Jeremy J. Jackson,[†] Christopher M. Rouleau,[†] Gyula Eres,[‡] and Karren L. More[‡]

[†]Center for Nanophase Materials Sciences and [‡]Materials Science and Technology Division, Oak Ridge National Laboratory, Oak Ridge, Tennessee 37831-6488, United States

ABSTRACT The nucleation and growth kinetics of single-wall carbon nanotubes in aligned arrays have been measured using fast pulses of acetylene and *in situ* optical diagnostics in conjunction with low pressure chemical vapor deposition (CVD). Increasing the acetylene partial pressure is shown to decrease nucleation times by three orders of magnitude, permitting aligned nanotube arrays to nucleate and grow to micrometers lengths within single gas pulses at high (up to 7 μm/s) peak growth rates and short ~0.5 s times. Low-frequency Raman scattering (>10 cm^{-1}) and transmission electron microscopy measurements show that increasing the feedstock flux in both continuous- and pulsed-CVD shifts the product distribution to large single-wall carbon nanotube diameters >2.5 nm. Sufficiently high acetylene partial pressures in pulsed-CVD appear to temporarily terminate the growth of the fastest-growing, small-diameter nanotubes by overcoating the more catalytically active, smaller catalyst nanoparticles within the ensemble with non-nanotube carbon in agreement with a growth model. The results indicate that subsets of catalyst nanoparticle ensembles nucleate, grow, and terminate growth within different flux ranges according to their catalytic activity.

KEYWORDS: single wall carbon nanotubes · chemical vapor deposition · induction time · nucleation · growth rate · kinetics · *in situ* · real-time · diagnostics · pulsed growth · diameter distribution · flux · aligned · partial pressure

Despite the intense interest in the controlled growth of single-wall carbon nanotubes (SWNTs) by chemical vapor deposition, several long-standing questions remain about how ensembles of catalyst nanoparticles respond to processing variables such as temperature, choice of hydrocarbon feedstock gas, gas flux, and partial pressure. Factors controlling the nucleation efficiency, diameter, wall number, and chirality of nanotubes remain critical not only for nanoscale electronics, where individual nanotubes are desired, but also in vertically aligned nanotube forests, where more macroscopic properties are developed, such as electrical conductivity for interconnects[1,2] and thermal conductivity for thermal interface materials.[3,4] High areal densities of catalyst nanoparticles contain a variety of particle sizes and compositions yet often exhibit a cooperative response in the growth and termination of dense nanotube forests of uniform lengths, the mechanisms for which remain key questions.[5−8]

Although a variety of effects can affect nanotube diameter and quality, including catalyst composition,[9,10] type of feedstock gas,[11−13] and effects of oxidant or inert background gases on catalyst shape,[10,14,15] the partial pressure of carbon feedstock gas has also been shown to play a major role.[16−18] In seminal work, Cheung et al. showed not only that catalyst nanoparticle size governs the diameter of resultant nanotubes but also noted the important role that reactant partial pressure plays to determine the distribution of nanotube diameters that grow from an ensemble of polydisperse particles.[16] Larger diameter nanoparticles were shown to require higher partial pressures to nucleate and grow correspondingly larger diameter nanotubes. Later, Lu et al. showed that by lowering not only the carbon feeding rate but also the temperature, small diameter (<1 nm) SWNTs could selectively be grown from a wide distribution of catalyst nanoparticle diameters and proposed an optimal carbon feeding rate to grow SWNTs from different diameter nanoparticles, with overfed nanoparticles shutting down growth due to overcoating with carbon and underfed particles never nucleating.[17,19]

The rapid growth of SWNTs in millimeters-long aligned arrays[20] tends to result in large-diameter nanotubes with a broad distribution of diameters (*e.g.*, 1−5 nm, average of 3.0 nm).[21] Raman spectroscopy of vertically aligned carbon nanotube arrays (VANTA) typically indicate much higher fractions of small-diameter SWNTs and higher *G*:*D* band ratios for the nanotubes grown earliest (in the top portion of the arrays), indicating that the nanotube diameters or wall-numbers (as well as defect levels), are changing with time during growth.[11,22]

* Address correspondence to geohegandb@ornl.gov.

Received for review August 9, 2011 and accepted September 3, 2011.

Published online September 15, 2011
10.1021/nn2030397

However, the accurate analysis of wall number and SWNT fraction in such arrays is difficult to characterize by Raman spectroscopy because most Raman instruments are sensitive only to ~100 cm^{-1} from the laser frequency, limiting the assessment of SWNTs diameters to <2.5 nm. Recently, Hasegawa et al. used TEM analysis to confirm a doubling in the average SWNT diameter (from ~1.5 to 3 nm) during the first 200 μm of rapid SWNT array growth for several acetylene partial pressures.[23]

To understand the prolonged growth of carbon nanotubes in aligned arrays for different fluxes and temperatures, we developed a combined approach utilizing time-resolved, *in situ* optical diagnostics[5,11,22,24,25] of nanotube array growth kinetics and an associated growth model.[25,26] Our growth model was based upon the concepts of Baker,[27] as were those of many other researchers[28−30] to explain the growth of both nanofibers and nanotubes. It predicts the growth kinetics, number of walls, and terminal length of nanotubes grown for a particular catalyst preparation at different hydrocarbon fluxes and temperatures.[25] It also predicts that the fastest growing nanotubes are SWNTs and determines the optimal hydrocarbon flux for fast SWNT growth from catalyst nanoparticles of different activities.[26] In the model, growth of a nanotube terminates when surface carbon forms faster from decomposed feedstock than it can be removed by dissolution into the particle or by surface diffusion to the growing nanotube.

Recently, we explored the growth of VANTAs by pulsed CVD and showed that the rapid variations in carbon supply inherent to the process can produce variations in the density of nanotube arrays, permitting the construction of multilayered nanotube architectures with variable density and layer spacing.[31] In pulsed CVD, the feedstock gas is supplied by a pulsed valve, and fast flows of background gases at low pressures carry the hydrocarbon gas past the substrate within discrete time periods.[31] Pulsed CVD differs in two main respects from conventional CVD: First, the growth of the array is interrupted by stops and starts, requiring repeated continuation or renucleation of growth on catalyst nanoparticles.[32] Second, the flux of feedstock varies over a wide range during a brief period. Fundamentally, pulsed CVD thereby provides a means not only to understand the kinetics of nanotube nucleation, renucleation, and growth but also to explore how rapidly ensembles of active sites can respond to highly nonequilibrium growth conditions.

Here, we explore the effects of changing acetylene partial pressure on the growth kinetics and diameter distribution of nanotubes in VANTAs grown by both constant flows and pulsed CVD. At low total pressures, where fast gas flows and optical diagnostics provide ~0.1 s time resolution for kinetics studies, increasing the hydrocarbon partial pressure is shown to markedly decrease the nucleation time for coordinated array growth as well as terminate the growth of small-diameter SWNTs, selectively producing large-diameter SWNT arrays. Interrupting the growth and reducing the acetylene flux is shown to reinitiate small-diameter SWNTs in the arrays. These results, taken together with recent TRR measurements of density variations in VANTAs[31] and growth model considerations, provide a more complete picture of their coordinated growth.

EXPERIMENTAL SECTION

TRR is a sensitive technique to measure the height and the density of VANTAs during the first 20 μm of their growth.[5,24,25,31] Fabry−Perot interference oscillations in the signal amplitude indicate aligned growth, and each fringe corresponds to an additional ~300 nm increase in height. Recently, we showed that the effective extinction coefficient obtained from the exponential attenuation of the TRR signal is directly proportional to the density in the VANTA array, even for layered VANTAs with oscillating density variations as large as a factor of 1.6.[31] Therefore, TRR can be used to simultaneously understand how both the density and the growth rate of a VANTA evolve with variations in growth conditions.

The experimental apparatus used for the pulsed CVD growth of VANTAs has been described elsewhere.[31] All experiments described here used a 0.5 nm Fe catalyst and 30 nm Al_2O_3 buffer layer on Si wafers at 690−720 °C within a conventional 3 inch o.d. tube furnace into which Ar (2000 sccm) and H_2 (250 sccm) gases are continuously flowed at low (6.3 Torr) pressure. Pulses of acetylene were introduced into this fast-flowing Ar/H_2 mixture with a pulsed valve upstream of the quartz tube. Modeling of the pulse of acetylene arriving at the vertically standing substrate 0.6 m away predicts a pulse width full-width at half-maximum (fwhm) of ~0.12s after a transit delay of ~0.1s. The transients in the optical reflectivity signal measured experimental fwhm pulse widths of 0.2−0.25 s fwhm, however. For the pulsed growth experiments described here, the volume of acetylene gas injected per pulse at 20 °C ranged from 0.2 to 3.1 cm^3, providing peak fluxes (using a 0.2 s fwhm acetylene pulse) of ~0.53−8.2 × 10^{18} $cm^{-2}s^{-1}$ which are equivalent to 60−920 sccm continuous acetylene flows at 6.3 Torr. After each pulse, 10 s of time was provided before the next pulse to ensure that growth had stopped.

After growth, the nanotube arrays on Si substrates were typically cleaved at a position that included the optically monitored spot and investigated from the side by scanning electron microscopy (Hitachi S-4700 FEG-SEM at ~2 kV). Strips of the array from the cleaved region were transferred to TEM grids for analysis by either Z-contrast scanning TEM (STEM) (Hitachi HD-2000 at 200 kV) or bright field TEM imaging (Hitachi HF-2000 at 200 kV). Raman spectroscopy capable of measuring large-diameter SWNTs grown in VANTAs was performed on the sides of the cleaved arrays using a Jobin-Yvon T-64000 triple monochromator system and 532 nm laser excitation.[33]

RESULTS AND DISCUSSION

VANTAs with banded appearance were grown by pulsed CVD as shown in Figure 1a−c. The nanotubes grow by base growth, each band corresponding to a separate pulse of gas, with the band corresponding to the first gas pulse located at the top of the array. The

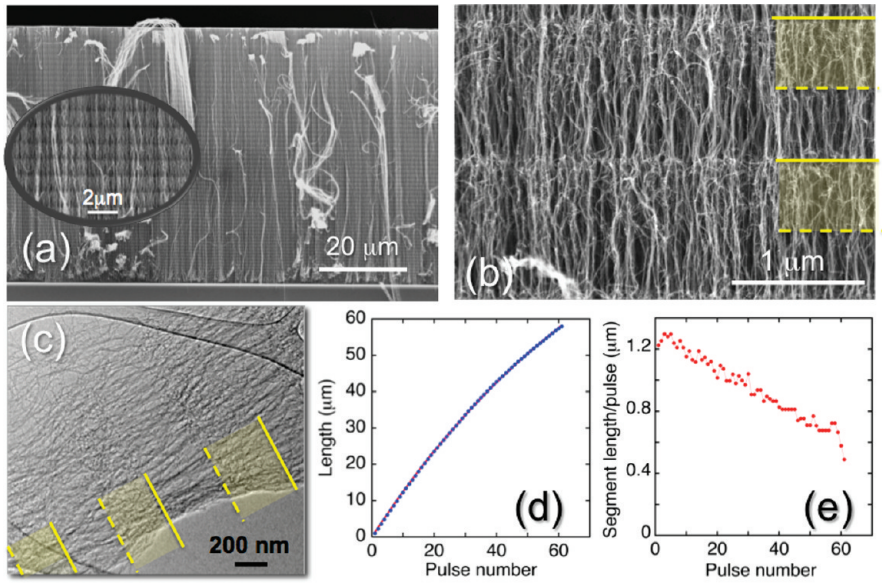

Figure 1. (a) Side-view SEM image of cleaved VANTA formed from 62 equal pulses of acetylene (each equivalent to 570 sccm for 0.2 s) into flowing Ar/H_2 at 690 °C, showing banded appearance. (b) Closer view SEM image of two bands in the array, corresponding to two gas pulses. Disordered nanotubes (adding to aligned nanotubes running throughout the array) in the denser portion of each band are indicated in the yellow-shaded zones, corresponding to the early, high-flow portion of each gas pulse. (c) TEM image of a strand of the array shows another view of the disordered zones. (d) Evolution of the array length *vs* pulse number. (e) Length of each band as a function of pulse number in the array.

bands provide a record of the incremental growth of the array for each subsecond acetylene pulse.[34] Corresponding estimates of the increase in array length per pulse using Fabry–Perot interference oscillations measured by *in situ* TRR (not shown) yielded excellent agreement with the lengths of the bands measured *ex situ via* SEM.

As shown in ref 31, TRR measurements and Z-contrast STEM revealed that the density of nanotubes within each band varies, with a sub-band of disordered crossbar nanotubes appearing in the high-density region of each band. The bright contrast difference in the SEM micrographs is due to this disordered layer of nanotubes within each growth band (yellow-shaded region in Figure 1b). Strips of the arrays that were loosened by the cleavage process were placed onto TEM grids, as described in ref 31. TEM images of the strips (Figure 1c) confirm that this band of disordered nanotubes occurs at the beginning of each gas pulse and that these crossbar nanotubes are interwoven within a distribution of vertically aligned carbon nanotubes which appear to run continuously throughout the array from band to band.

As shown in Figure 1d and e, the length of each band decreases linearly as a function of pulse number, resulting in a decline in the growth rate of the array. Such rolloffs in growth efficiency are not unique to pulsed CVD. The length of continuously grown nanotube arrays, for example, can be fit by $L(t) = \beta\tau(1 - \exp(-t/\tau))$ relating length, L, to time, t, and the initial growth rate, β, and the catalyst lifetime, τ.[25,35–37] In our previous work we found that the density of VANTAs also progressively declines from the top to the bottom of the array, both for continuous growth from constant feedstock flux and for pulsed growth from varying flux.[31] Such long-term declines in the growth rate and the density of nanotube arrays have been attributed to many factors, including Ostwald ripening,[38] diffusion-limited feedstock supply,[36,39,40] diffusion of the catalyst into the support,[41] catalyst poisoning,[42] or collective mechanical effects.[6]

Here, performing CVD with fast gas pulses of acetylene, we investigate how the growth rate and the composition of the nanotube array are affected by rapid variations in the partial pressure of acetylene on very short time scales compared to these long-term declines. Figure 2 shows subsecond growth kinetics of a nanotube array for the first three pulses. The growth rates *within each gas pulse* were calculated from the spacing between Fabry–Perot fringe maxima and minima in the time-resolved reflectivity (TRR) signal (refs 25 and 31 and Supporting Information). Here, $t = 0$ corresponds to the time measured at the onset of growth on the first gas pulse (where the TRR signal deflects from a constant value) and therefore occurs after the transit time of gas to the substrate as well as the nucleation time for growth on the first pulse. The subsequent $t = 0$ times for the second and third pulses in Figure 2 follow exactly 10 and 20 s after $t = 0$ for the first gas pulse, since the pulsed valve is fired precisely at 0.100 Hz. The peak growth rate within the first pulse is extremely high, reaching 7.3 μm/s at 0.1 s after growth begins. The growth rate falls to 3 μm/s at the tail of the pulse, resulting in a total array length of

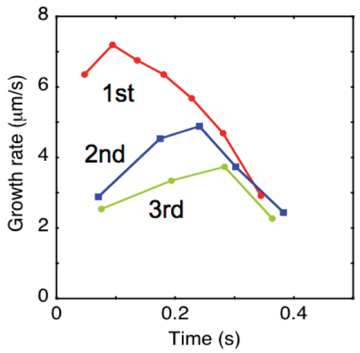

Figure 2. (a) Instantaneous growth rates measured from TRR during the first three pulses of array growth (pulse estimated 570 sccm and 0.2 s half-width).

2.2 μm for the first pulse of gas. However, the peak growth rate on the second and third pulses declines (to 4.9 and 3.6 μm/s, respectively) and shifts to later in the gas pulse (at t = 0.24 and 0.28 μs, respectively), ending with very similar growth rates at the end of the three pulses.

As shown in ref 31, each successive band declines slightly in length, and its peak density declines also, reflecting a decrease in overall catalytic activity. However, the kinetics data of Figure 2 indicate that the fastest growing nanotubes in the high-partial pressure portion of the pulse are preferentially declining compared to slower growing nanotubes later within each pulse.

To understand the nature of the fastest-growing nanotubes at high acetylene partial pressures, single-pulse growth experiments were performed. Figure 3a shows a side-on SEM image of a cleaved, 1.3 μm tall nanotube array grown by a single gas pulse. Strips from the side of the cleaved array were deposited on TEM grids for analysis, as shown in Figure 3b. This array was nearly finished its growth within 0.5 s, as indicated by the TRR signal in Figure 3c, which exhibits ~4 oscillations in the reflectivity, each corresponding to ~0.3 μm of growth. High-resolution TEM (HRTEM) images of the top and bottom regions of the array are given in Figure 3d and e. At the top of the array, highly disordered, tangled, defective nanotubes are observed along with disordered carbonaceous products. Both single- and double-wall carbon nanotubes were observed, in a variety of diameters between 0.5 and 6 nm. At the bottom of the array, corresponding to material that grew at the end of the first pulse of gas, aligned bundles of only large-diameter (2.5 – 6 nm) SWNTs were observed. In contrast to the top of the array, the SWNTs at the bottom of the array had well-formed, much less-defective walls along with a much lower density of non-nanotube carbon.

Therefore, highly defective nanotubes with a broad diameter distribution are responsible for the rapid array growth during the first half of the first gas pulse in the kinetics data of Figure 2. This component of fast-growing, defective nanotube material decreases on the second and third pulses, resulting in aligned single-wall nanotubes with large diameters and better wall quality. The small (1–2 nm) diameter SWNTs observed in TEM micrographs at the top of the array disappear within the first few gas pulses. Their catalyst particles either become deactivated more quickly on each pulse of gas or are permanently deactivated and do not renucleate.

Diameter distributions and wall numbers of nanotubes grown by pulsed-CVD with different peak acetylene fluxes were performed by examining HRTEM images of thin strands of nanotube arrays that had been cleaved. The nanotubes were nearly entirely SWNTs, with <1% double-wall nanotubes. One hundred SWNTs from different locations within long strands grown from multiple pulses were measured from HRTEM micrographs for different pulsed partial pressures. Two different pulsed valves were employed to provide a wide range of estimated peak acetylene partial pressures equivalent to continuous flows of 36–1230 sccm at 6.3 Torr but for just 0.2 s. For the high flows (570–1230 sccm) provided by the larger valve, a truncated diameter distribution was obtained compared to the flows (36–81 sccm) provided by the smaller valve. Figure 4 summarizes the observations for two cases: (a) low (60 sccm) and (b) high (920 sccm) peak acetylene flow. As shown in Figure 4a, the comparatively low-flow pulses displayed a much broader diameter distribution of SWNTs than high-flow pulses. SWNTs in the 0.5–2.5 nm range were nearly absent in arrays grown from the high-flow pulses. The important implication is that higher acetylene partial pressures attained within the gas pulses used for pulsed growth shift the product distribution to large diameters.

In order to check this conclusion, a series of separate continuous-feedstock growth experiments were performed at different acetylene flow rates for the same Ar/H_2 flows and 6.3 Torr total pressure used in the pulsed CVD experiments. As shown in the HRTEM image and diameter distribution of Figure 5a and b, for low 1–5 sccm acetylene flows entirely SWNTs (<1% DWNTs) with a broad distribution of diameters are found, with most nanotubes observed with 0.6–4 nm diameters and very few large-diameter (4–6 nm) nanotubes. As the acetylene partial pressure is raised, however, the diameter distribution shifts to favor larger diameter SWNTs and suppresses the smaller diameter SWNTs, as shown in Figure 5c and d for the 40 sccm C_2H_2 flow condition.

Representative microRaman spectra measured from the sides of cleaved arrays using 1.5 μm beam spot sizes are shown in Figure 6. These spectra include the low (10–125 cm^{-1}) frequency region and confirm the collapse of the SWNT product distribution to large-diameter nanotubes at higher acetylene partial pressures. In both the 40 sccm continuous flow and pulsed CVD (920 sccm peak

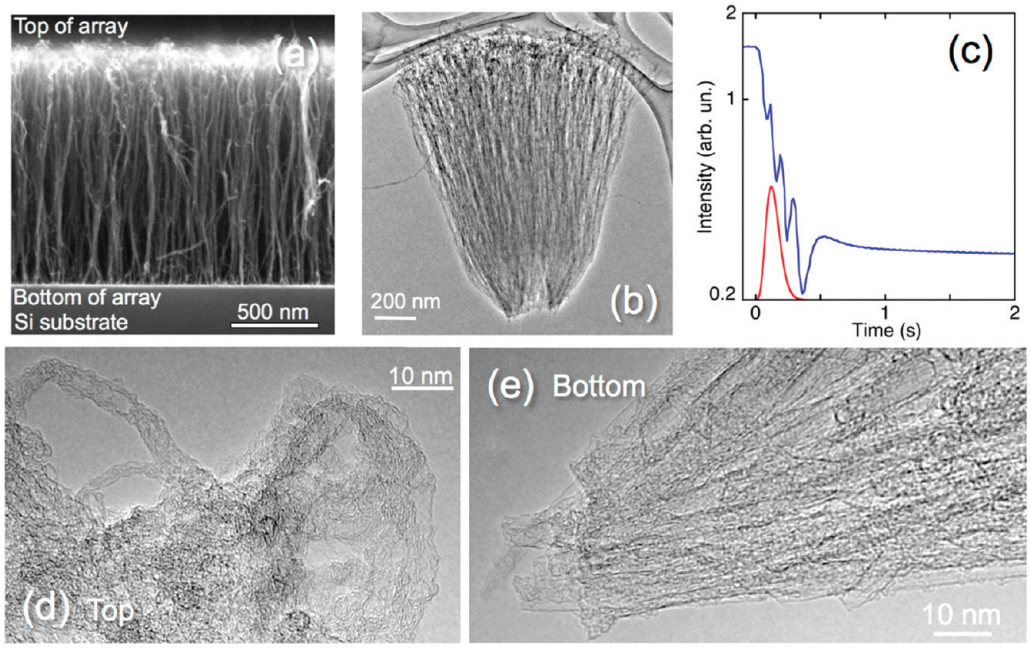

Figure 3. (a) Side-on SEM micrograph of a 1.3 μm tall, cleaved, vertically aligned nanotube array grown by a single pulse of gas (equivalent to 900 sccm for 0.2 s fwhm). (b) Corresponding TEM image of a tuft of the same array. (c) Optical reflectivity signal (blue) indicating the subsecond growth kinetics of the aligned array and temporal profile of acetylene partial pressure at substrate (red) after arrival at $t = 0$. (d) HRTEM image of the disordered carbon nanotubes at the top of the array. (e) HRTEM image of the aligned, large-diameter SWNTs at the bottom of the array.

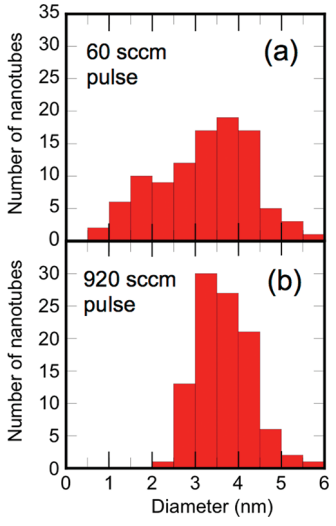

Figure 4. SWNT diameter distributions from HRTEM micrographs of strands taken from aligned nanotube arrays grown by repeated pulsing with peak acetylene fluxes of (a) 60 and (b) 920 sccm.

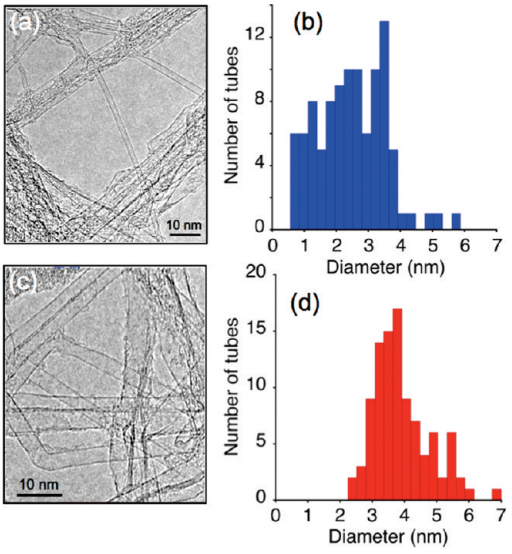

Figure 5. (a) TEM and (b) resulting histogram of diameters for SWNTs grown at 1−5 sccm acetylene flow. (c) TEM and (d) resulting histogram of SWNT diameters grown at 40 sccm acetylene flow.

flow) cases, breathing modes the 40−125 cm^{-1} region of the Raman spectra shown in Figure 6a indicate the presence of SWNTs in these arrays with diameters between 2 and 6 nm, in accordance with the TEM observations of Figures 4b and 5d. In addition, the SWNTs in these arrays are more defective compared to those grown at lower acetylene partial pressures, as evidenced by their relatively larger *D* bands shown in Figure 6b.

However, as shown in Figure 6a, at lower acetylene partial pressures Raman scattering intensity in the >125 cm^{-1} region emerges, while the intensity in the 40−125 cm^{-1} frequency region systematically decreases, indicating the presence of significant numbers of small (<2 nm) diameter SWNTs and fewer large diameter (2−6 nm) SWNTs. For 10 sccm acetylene flow, a broad distribution of both large- and small-diameter

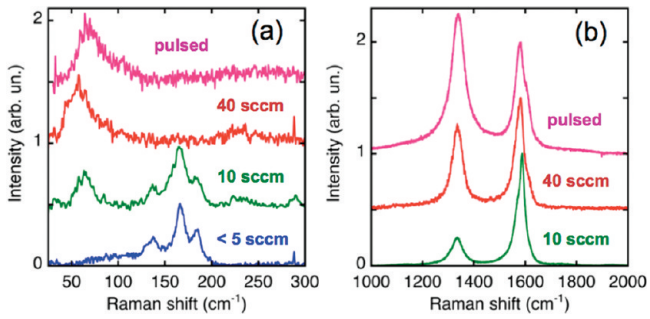

Figure 6. Raman spectra (λ_{ex} = 532 nm) of VANTAs grown under different continuous (CW) flows (<5−40 sccm) and pulsed flows (est. 570 sccm peak flow for 0.2 s). The breathing mode region in (a) shows a loss of small-diameter nanotubes in the >125 cm^{-1} region with increasing acetylene flux and a corresponding emergence of large-diameter nanotubes in the <125 cm^{-1} region. A corresponding increase in the *D vs* the *G* bands with increasing flux is observed in Raman scattering at higher frequencies in (b).

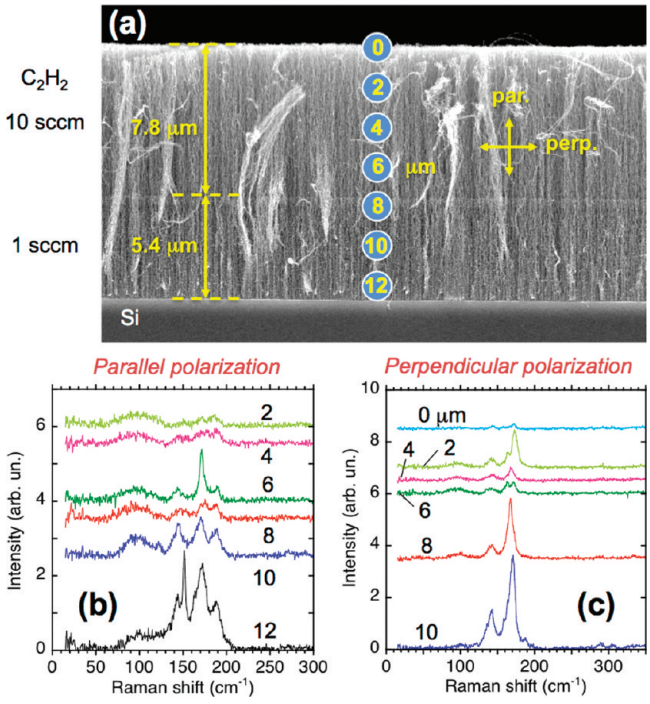

Figure 7. (a) SEM image of a cleaved cross-section of an aligned carbon nanotube array grown first at 10 sccm C_2H_2 gas, then after a 10 s pause, at 1 sccm C_2H_2 gas, along with the indicated points for Raman spectroscopy in the breathing mode spectral region for SWNTs at the indicated positions for the laser polarized (b) parallel and (c) perpendicular to the growth direction.

SWNTs are growing at the same time. However for acetylene flows <5 sccm, the distribution of SWNT diameters shifts to smaller (1.2−4 nm) diameters in agreement with the TEM measurements of Figure 5a.

Therefore, the data indicate that increasing hydrocarbon flow can shift the nanotube diameter distribution toward large-diameter SWNTs in these arrays. However, while SWNT diameter changes in long VANTAs may occur over hundreds of micrometers length and hundreds of seconds time during continuous growth,[11,22,23] the higher hydrocarbon partial pressures in pulsed growth appear to deactivate the smaller catalyst nanoparticles within just a few pulses. The arrays grown by pulsed CVD with high peak flow rates (this work and ref 31) exhibit cyclical density variations, which indicate that a fraction of the catalyst nanoparticle ensemble may be renucleating, growing, and terminating the growth of nanotubes within each subsecond pulse.

In order to understand whether catalyst nanoparticles that are deactivated by one flow condition can grow SWNTs again under different flow conditions, interrupted growth experiments using different continuous acetylene flow rates were performed. The array shown in Figure 7, for example, was grown first with 10 sccm acetylene flow for 100 s and then again with 1 sccm for 5700 s. Between the two flow conditions, the acetylene flow was turned off for 10 s to simulate the time period between pulses of gas in the pulsed growth experiments. Due to the high flow velocity

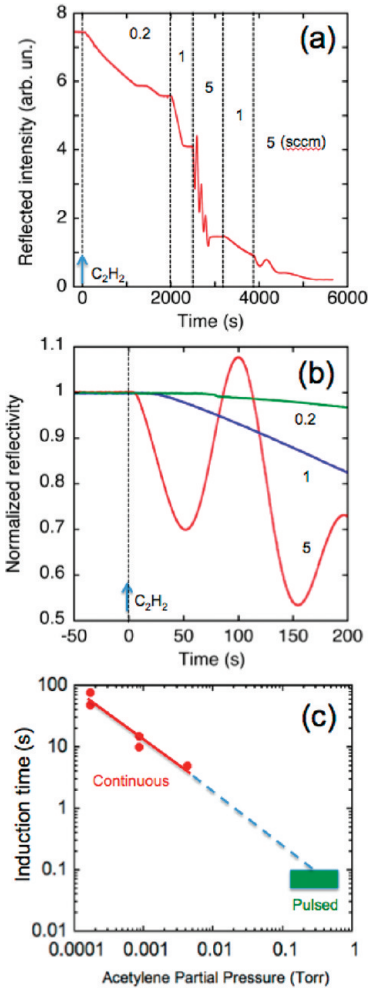

Figure 8. (a) *In situ* TRR signal during VANTA growth for 5 different C_2H_2 flows (in sccm). Growth was stopped for 10s before each new flow was introduced. (b) Normalized TRR signals following the introduction of acetylene (at $t = 0$ in each case) for three different flows (0.2, 1.0, and 5.0 sccm), showing different times for the onset of measurable deposition. (c) Plot of the induction times for the continuous flows of (a and b) in red and the estimated range of peak flows measured in pulsed growth experiments (green region), scaled in terms of acetylene partial pressure at 700 °C.

through the tube furnace at the low (6.3 Torr) pressures and high (2250 sccm) background Ar/H_2 flows used in these experiments, this time was sufficient to stop the growth of the array. The entire experiment was monitored with TRR (see Supporting Information). Raman spectra measured in the 10 sccm region (top 7.8 μm) of the array (see Figure 7b) were similar to the 10 sccm spectrum shown in Figure 6a, with a broad distribution of breathing modes across both the 40−125 and 125−210 cm^{-1} frequency regions. Raman spectra measured from the 1 sccm (lower 5.4 μm) portion of the array (see Figure 7b and c) indicate the strong re-emergence of small diameter ($d < 2$ nm, $\omega > 125$ cm^{-1}) SWNTs and a loss of large diameter SWNTs ($d > 3.5$ nm, $\omega < 70$ cm^{-1}). Although it is clear that portions of the array are always dislodged during the cleavage process (as shown in Figure 7a), lending some uncertainty to such position-dependent Raman measurements, similar line scans up and down other cleaved portions of the same array confirmed this recovery of smaller diameter SWNTs in the nanotube diameter distribution due to the reduction in acetylene partial pressure.

To understand the dependence of the induction time for the initiation of array growth on the acetylene partial pressure, we used a similar interrupted growth approach. Figure 8a shows a growth run where acetylene was gently introduced at 0.2 sccm into a background gas flow [Ar (2000 sccm), H_2 (250 sccm), 6.3 Torr] at $t = 0$, and then a series of five growth stoppages (for 10 s at the dashed lines) were implemented, followed by the gentle reintroduction of acetylene flow at 0.2, 1, or 5 sccm. After each growth stoppage, the induction time before the resumption of growth (signaled by the deflection of the reflectivity signal) was measured for each flow rate.

Figure 8b shows an expanded view of the normalized reflectivities for the first three growth periods, where $t = 0$ refers to the reintroduction of C_2H_2 in each case. Clearly, the induction times decrease with increasing acetylene partial pressure, from 76 s for 0.2 sccm flow to 25 at 1 sccm and to 10 at 5 sccm. In addition, the original nucleation of measurable array growth occurred after 76 at 0.2 sccm. However after stopping growth for 10 s, the induction time for regrowth at 0.2 sccm occurred after just 49 s. Similarly, the induction time for the second regrowth at 1 sccm decreased (*i.e.* 10 s *vs* 15 s).

Figure 8c plots these induction times as a function of the acetylene partial pressure at 700 °C for the different continuous flows of Figure 8a and b and the estimated peak pulsed flows. In all of the pulsed CVD experiments described here, the induction time for array growth was less than 0.1 ± 0.05 s, which represents the propagation time of the gas to the substrate and consideration for all timing errors under these low-pressure, fast-flow conditions.

The combined data of Figure 8c span three orders in magnitude in acetylene partial pressure and show a corresponding 3 orders of magnitude reduction in the induction time for nanotube array growth as the acetylene partial pressure is increased. As demonstrated above, it is reasonable to expect that the induction time will change as the nanoparticle catalytic activity changes throughout a growth run (or following stoppage of growth), altering the activation energies for dissociation of acetylene and dissolution of carbon by the catalyst nanoparticles. The induction time is also strongly dependent on the growth temperature and the choice of substrate, as recent *in situ* Raman spectroscopy measurements have demonstrated.[43] We measured a similar decrease in induction time *vs* flux for low-pressure, continuous acetylene beam growth in a cold wall reactor, however at higher fluxes.[7] In

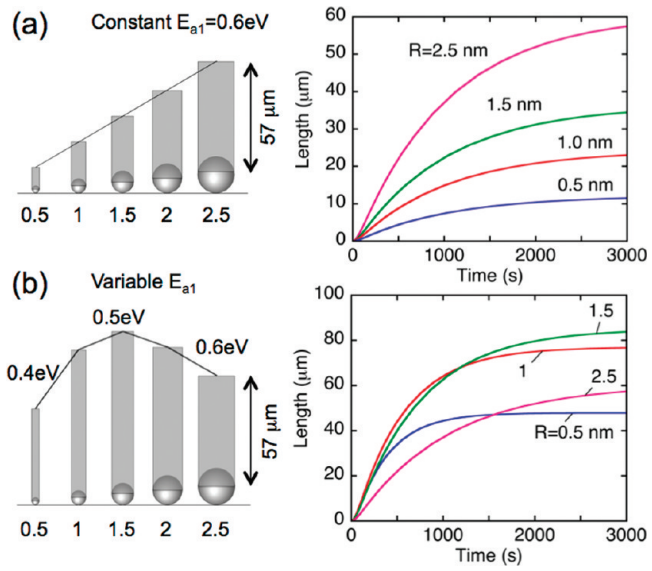

Figure 9. Nanotube height distributions (terminal lengths) and kinetics of growth from catalyst nanoparticles of different radii predicted by the model in ref 31 with activation energies E_{a_1} and E_{a_2} for the catalytic decomposition and dissolution of feedstock gas, respectively. (a) Both E_{a_1} = 0.6 eV and E_{a_2} = 0.7 eV are constant for all particles, and nanotubes grow at different rates, and terminate at different lengths. (b) E_{a_1} is variable, and E_{a_2} = 0.7 eV results in more uniform growth rates and terminal lengths.

pulsed CVD, sufficiently high effective partial pressures can shorten the induction time to permit highly effective growth within the time constraints of a gas pulse.

The coordinated growth of VANTAs implies a diameter-dependent variation in the catalytic activity of nanoparticles. As shown in Supporting Information and illustrated in Figure 9a and b, it follows from our previous growth model that if catalyst nanoparticles with different radii had equal catalytic activity (expressed in terms of the activation energies E_{a_1} and E_{a_2} for the catalytic decomposition and dissolution of feedstock gas, respectively),[25] the larger diameter nanotubes should grow faster than the smaller diameter nanotubes due to their higher surface area to circumference ratio. In this case, the coordinated growth of long VANTAs with the observed broad diameter distributions would be difficult to explain. Moreover, the growth model predicts that for particles with equal catalytic activity, the nanotubes from smaller nanoparticles should terminate growth at much shorter lengths for a given feedstock flux than nanotubes grown from larger particles, due to carbon overcoating or other catalyst poisoning mechanisms (model predictions plotted in Figure 9a).

In order for a broad distribution of catalyst nanoparticle diameters to grow nanotubes with corresponding diameters at nearly equal rates and to terminate growth at similar lengths, the catalytic activity must be varied in the growth model as a function of nanoparticle diameter. Specifically, the smaller nanoparticles must have a lower activation energy E_{a_1} (more catalytically active for dissociation of the feedstock) in the example of Figure 9b for their growth rate to keep pace with that of the larger nanoparticles. However if the dissolution and/or the surface diffusion rates of carbon on the nanoparticle are not also increased, the model predicts that the overproduction of carbon on the surface of the nanoparticle will lead to its overcoating and cessation of growth. This situation is consistent with the observed narrowing of the diameter distributions at higher acetylene partial pressures.

CONCLUSIONS

In situ kinetics measurements during the pulsed and continuous growth of VANTAs at low pressure were correlated with *ex situ* Raman spectroscopy, HRTEM, and Z-STEM characterization of the nanotube diameters, products, and density to provide new understanding of the effects of feedstock partial pressure on catalyst nanoparticle ensembles for nucleation, growth, and deactivation. Pulsed growth with peak flow rates >570 sccm (corresponding to just 1.3 Torr acetylene partial pressure, however) effectively eliminates the growth of SWNTs with diameters <2.5 nm, shifting the distribution into the 2−6 nm range, as detected by a broad Raman scattering band in the 40−125 cm^{-1} frequency range. Similar shifts in the diameter distribution were obtained for VANTAs grown with continuous acetylene flow at 40 sccm (0.11 Torr partial pressure acetylene).

The results indicate that subsets of catalyst nanoparticles in typically prepared ensembles nucleate, grow, and terminate in different ranges of feedstock partial pressure according to their catalytic activity. This result is consistent with our previously published growth model that simulated the slowing and termination of growth of a nanotube by the loss in surface

area and eventual overcoating of its corresponding catalyst nanoparticle. Here we considered the effects of diameter-dependent catalytic activity and showed that smaller nanoparticles should have greater catalytic activity in order for small-diameter nanotubes to keep pace with large-diameter nanotubes in the coordinated growth of aligned arrays of broad diameter distribution.

In pulsed CVD, each gas pulse rapidly sweeps the feedstock flux at a catalyst nanoparticle surface over a wide range, permitting the response of the catalyst nanoparticle ensemble to changing flux to be partly separated from long-term changes in the activity, density, or disappearance of the catalyst. Within a single subsecond pulse of gas, HRTEM images of the resulting layer revealed that only large diameter SWNTs were able to survive the high-flux portion of the gas pulse, with smaller diameter nanotubes and other highly disordered nanotubes of various diameters apparently extinguished in carbonaceous byproducts, consistent with the aforementioned carbon overcoating mechanism for more catalytically active, smaller nanoparticles. This disordered region of both small- and large-diameter nanotubes at the top of the array is responsible for the fastest (initial) growth of the array on the first pulse, associated kinetics measurements showed. The active nanoparticles on the second and third pulses have less catalytic activity, producing significantly shorter lengths per pulse with progressively more uniform growth rates throughout the pulse, indicating that the fastest-growing component of the nanoparticle ensemble may remain inactive on subsequent pulses.

Stopping the growth and allowing the catalyst a 10 s rest between pulses can repeatedly recover a significant fraction of the peak density from the previous pulse, producing the banded appearance in the arrays. The fraction of regenerable catalyst nanoparticles may be roughly estimated from the density extrapolations measured for the disordered bands in the pulsed CVD arrays (*e.g.*,∼ 25% in Figure 3c of ref 31). This indicates that not all of the nanoparticles are irreversibly overcoated, lost, or poisoned by the previous pulse. In the context of our growth model, these catalyst nanoparticles may dissolve their carbonaceous overcoat layer once the carbon deposition due to the feedstock gas stops. As shown in Figure 7 for continuous flows at low partial pressures, even small-diameter catalyst nanoparticles can recover to grow small-diameter nanotubes again if they are not irreversibly overcoated. Thus, the kinetics of this dissolution process during the rest period inherent to pulsed growth implies that the distribution of diameters in the array, as well as the array density, may be tunable through the choice of repetition rate as well as the hydrocarbon partial pressure in pulsed growth.

It is also reasonable to expect that the catalytic activity varies among catalyst nanoparticles not only as a function of nanoparticle diameter but also among those particles sharing a given nanoparticle diameter (*e.g.*, resulting from variations in particle composition and crystalline structure and from interaction with the catalyst support). In this case, the wide variation in acetylene partial pressure within gas pulses in pulsed CVD might result in the repeated termination of the more catalytically active subset of nanoparticles within a distribution of regenerable particles, explaining the density variations observed in the banded VANTAs of pulsed CVD.[31]

Finally, time-resolved measurements show that induction times for VANTA growth and regrowth decrease with increasing acetylene partial pressures and are extremely short for the high-peak fluxes used here for pulsed growth, within the <0.1 s range at the limit of our current gas delivery and modeling uncertainties. Such rapid, sub 0.1 s variations in both the density and the product distribution within the VANTA provide a new perspective on how quickly a catalyst ensemble can respond to changing growth conditions during CVD.

METHODS

Pulsed CVD of VANTAs. The experimental apparatus is generally described in ref 31. For pulsed growth Ar (2000 sccm) and H_2 (250 sccm) gases were flowed continuously, and acetylene gas was injected from one of two pulsed valves (Parker models: 099-0167-900 and 099-0340-900) using a 1.0 ms wide electrical pulse supplied by a digital delay generator (Stanford Research Systems, DG545), which was subsequently amplified. The amount of acetylene introduced per pulse depends on the backing pressure supplied to the pulsed valves (20−60 psi) and ranged from 0.2 to 3.1 cm^3 at 20 °C, as determined from pressure rises measured in a calibrated volume. All experiments were carried out at low (6.3 Torr) total pressure and ∼700 °C, so normal continuous growth (*e.g.* at 10 sccm acetylene) and the maximum peak fluxes used in these experiments (920 sccm acetylene in Figure 4) correspond to partial pressures of acetylene of only 28 mTorr and 1.8 Torr, respectively.

Optical Reflectivity Measurements. A continuous HeNe laser at 633 nm was used to illuminate a vertically standing substrate in the tube furnace. The specularly reflected beam was turned by a first surface mirror, passed through a lens and bandpass filter and digitized (12 bit) with a fast photodiode at 300 points/s.

Acknowledgment. Synthesis science sponsored by the Materials Sciences and Engineering Division, Office of Basic Energy Sciences, U.S. Department of Energy. Sample characterization by Raman spectroscopy at the Center for Nanophase Materials Sciences (CNMS) and electron microscopy at the Shared Research Equipment (SHaRE) User Facility sponsored at Oak Ridge National Laboratory by the Scientific User Facilities Division, Office of Basic Energy Sciences, U.S. Department of

Energy. We gratefully acknowledge the technical assistance of Pam Fleming.

Supporting Information Available: TRR data for the interrupted growth experiment and model predictions for growth rate and terminal lengths of SWNTs grown from nanoparticles with different diameters.This material is available free of charge *via* the Internet at http://pubs.acs.org.

REFERENCES AND NOTES

1. Robertson, J.; Zhong, G.; Telg, H.; Thomsen, C.; Warner, J. H.; Briggs, G. A. D.; Dettlaff-Weglikowska, U.; Roth, S. Growth and Characterization of High-Density Mats of Single-Walled Carbon Nanotubes for Interconnects. *Appl. Phys. Lett.* **2008**, *93*, 163111–163113.
2. Nihei, M.; Kawabata, A.; Kondo, D.; Horibe, M.; Sato, S.; Awano, Y. Electrical Properties of Carbon Nanotube Bundles for Future Via Interconnects. *Jpn. J. Appl. Phys., Part 1* **2005**, *44*, 1626–1628.
3. Huang, H.; Liu, C. H.; Wu, Y.; Fan, S. S. Aligned Carbon Nanotube Composite Films for Thermal Management. *Adv. Mater.* **2005**, *17*, 1652–1656.
4. Ivanov, I.; Puretzky, A.; Eres, G.; Wang, H.; Pan, Z. W.; Cui, H. T.; Jin, R. Y.; Howe, J.; Geohegan, D. B. Fast and Highly Anisotropic Thermal Transport through Vertically Aligned Carbon Nanotube Arrays. *Appl. Phys. Lett.* **2006**, *89*, 223110–223112.
5. Puretzky, A. A.; Eres, G.; Rouleau, C. M.; Ivanov, I. N.; Geohegan, D. B. Real-Time Imaging of Vertically Aligned Carbon Nanotube Array Growth Kinetics. *Nanotechnology* **2008**, *19*, 055605–055609.
6. Hart, A. J.; Bedewy, M.; Meshot, E. R.; Guo, H. C.; Verploegen, E. A.; Lu, W. Collective Mechanism for the Evolution and Self-Termination of Vertically Aligned Carbon Nanotube Growth. *J. Phys. Chem. C* **2009**, *113*, 20576–20582.
7. Eres, G.; Rouleau, C. M.; Yoon, M.; Puretzky, A. A.; Jackson, J. J.; Geohegan, D. B. Model for Self-Assembly of Carbon Nanotubes from Acetylene Based on Real-Time Studies of Vertically Aligned Growth Kinetics. *J. Phys. Chem. C* **2009**, *113*, 15484–15491.
8. Meshot, E. R.; Hart, A. J. Abrupt Self-Termination of Vertically Aligned Carbon Nanotube Growth. *Appl. Phys. Lett.* **2008**, *92*, 113107.
9. Kataura, H.; Kumazawa, Y.; Maniwa, Y.; Ohtsuka, Y.; Sen, R.; Suzuki, S.; Achiba, Y. Diameter Control of Single-Walled Carbon Nanotubes. *Carbon* **2000**, *38*, 1691–1697.
10. Hauge, R. H.; Pint, C. L.; Pheasant, S. T.; Parra-Vasquez, A. N. G.; Horton, C.; Xu, Y. Q. Investigation of Optimal Parameters for Oxide-Assisted Growth of Vertically Aligned Single-Walled Carbon Nanotubes. *J. Phys. Chem. C* **2009**, *113*, 4125–4133.
11. Eres, G.; Kinkhabwala, A. A.; Cui, H. T.; Geohegan, D. B.; Puretzky, A. A.; Lowndes, D. H. Molecular Beam-Controlled Nucleation and Growth of Vertically Aligned Single-Wall Carbon Nanotube Arrays. *J. Phys. Chem. B* **2005**, *109*, 16684–16694.
12. Saito, T.; Ohshima, S.; Okazaki, T.; Ohmori, S.; Yumura, M.; Iijima, S. Selective Diameter Control of Single-Walled Carbon Nanotubes in the Gas-Phase Synthesis. *J Nanosci. Nanotechnol.* **2008**, *8*, 6153–6157.
13. Xiang, R.; Einarsson, E.; Okawa, J.; Miyauchi, Y.; Maruyama, S. Acetylene-Accelerated Alcohol Catalytic Chemical Vapor Deposition Growth of Vertically Aligned Single-Walled Carbon Nanotubes. *J. Phys. Chem. C* **2009**, *113*, 7511–7515.
14. Harutyunyan, A. R.; Chen, G. G.; Paronyan, T. M.; Pigos, E. M.; Kuznetsov, O. A.; Hewaparakrama, K.; Kim, S. M.; Zakharov, D.; Stach, E. A.; Sumanasekera, G. U. Preferential Growth of Single-Walled Carbon Nanotubes with Metallic Conductivity. *Science* **2009**, *326*, 116–120.
15. Sumpter, B. G.; Meunier, V.; Romo-Herrera, J. M.; Cruz-Silva, E.; Cullen, D. A.; Terrones, H.; Smith, D. J.; Terrones, M. Nitrogen-Mediated Carbon Nanotube Growth: Diameter Reduction, Metallicity, Bundle Dispersability, and Bamboo-Like Structure Formation. *ACS Nano* **2007**, *1*, 369–375.
16. Cheung, C. L.; Kurtz, A.; Park, H.; Lieber, C. M. Diameter-Controlled Synthesis of Carbon Nanotubes. *J. Phys. Chem. B* **2002**, *106*, 2429–2433.
17. Lu, C. G.; Liu, J. Controlling the Diameter of Carbon Nanotubes in Chemical Vapor Deposition Method by Carbon Feeding. *J. Phys. Chem. B* **2006**, *110*, 20254–20257.
18. Hahm, M. G.; Kwon, Y. K.; Lee, E.; Ahn, C. W.; Jung, Y. J. Diameter Selective Growth of Vertically Aligned Single Walled Carbon Nanotubes and Study on Their Growth Mechanism. *J. Phys. Chem. C* **2008**, *11*, 17143–17147.
19. Li, Y.; Cui, R. L.; Ding, L.; Liu, Y.; Zhou, W. W.; Zhang, Y.; Jin, Z.; Peng, F.; Liu, J. How Catalysts Affect the Growth of Single-Walled Carbon Nanotubes on Substrates. *Adv. Mater.* **2010**, *22*, 1508.
20. Hata, K.; Futaba, D. N.; Mizuno, K.; Namai, T.; Yumura, M.; Iijima, S. Water- Assisted Highly Efficient Synthesis of Impurity-Free Single-Waited Carbon Nano- Tubes. *Science* **2004**, *306*, 1362–1364.
21. Futaba, D. N.; Hata, K.; Namai, T.; Yamada, T.; Mizuno, K.; Hayamizu, Y.; Yumura, M.; Iijima, S. 84% Catalyst Activity of Water-Assisted Growth of Single Walled Carbon Nanotube Forest Characterization by a Statistical and Macroscopic Approach. *J. Phys. Chem. B* **2006**, *110*, 8035–8038.
22. Geohegan, D. B.; Puretzky, A. A.; Styers-Barnett, D.; Hu, H.; Zhao, B.; Cui, H.; Rouleau, C. M.; Eres, G.; Jackson, J. J.; Wood, R. F.; Pannala, S.; Wells, J. C. In situ" Time-Resolved Measurements of Carbon Nanotube and Nanohorn Growth. *Phys. Status Solidi B* **2007**, *244*, 3944–3949.
23. Hasegawa, K.; Noda, S. Millimeter-Tall Single-Walled Carbon Nanotubes Rapidly Grown with and without Water. *ACS Nano* **2011**, *5*, 975–984.
24. Geohegan, D. B.; Puretzky, A. A.; Ivanov, I. N.; Jesse, S.; Eres, G.; Howe, J. Y. In situ" Growth Rate Measurements and Length Control During Chemical Vapor Deposition of Vertically Aligned Multiwall Carbon Nanotubes. *Appl. Phys. Lett.* **2003**, *83*, 1851–1853.
25. Puretzky, A. A.; Geohegan, D. B.; Jesse, S.; Ivanov, I. N.; Eres, G. In situ" Measurements and Modeling of Carbon Nanotube Array Growth Kinetics During Chemical Vapor Deposition. *Appl. Phys. A: Mater. Sci. Process.* **2005**, *81*, 223–240.
26. Wood, R. F.; Pannala, S.; Wells, J. C.; Puretzky, A. A.; Geohegan, D. B. Simple Model of the Interrelation between Single- and Multiwall Carbon Nanotube Growth Rates for the Cvd Process. *Phys. Rev. B* **2007**, *75*, 235446.
27. Baker, R. T. K.; Barber, M. A.; Waite, R. J.; Harris, P. S.; Feates, F. S. Nucleation and Growth of Carbon Deposits from Nickel Catalyzed Decomposition of Acetylene. *J. Catal.* **1972**, *26*, 51–62.
28. Chitrapu, P.; Lund, C. R. F.; Tsamopoulos, J. A. A Model for the Catalytic Growth of Carbon Filaments. *Carbon* **1992**, *30*, 285–293.
29. Safvi, S. A.; Bianchini, E. C.; Lund, C. R. F. The Dependence of Catalytic Carbon-Filament Growth-Kinetics Upon Gas-Phase Carbon Activity. *Carbon* **1991**, *29*, 1245–1250.
30. Alstrup, I. A New Model Explaining Carbon-Filament Growth on Nickel, Iron, and Ni-Cu Alloy Catalysts. *J. Catal.* **1988**, *109*, 241–251.
31. Jackson, J. J.; Puretzky, A. A.; More, K. L.; Rouleau, C. M.; Eres, G.; Geohegan, D. B. Pulsed Growth of Vertically Aligned Nanotube Arrays with Variable Density. *ACS Nano* **2010**, *4*, 7573–7581.
32. Kawarada, H.; Iwasaki, T.; Robertson, J. Mechanism Analysis of Interrupted Growth of Single-Walled Carbon Nanotube Arrays. *Nano Lett.* **2008**, *8*, 886–890.
33. Puretzky, A. A.; Geohegan, D. B.; Rouleau, C. M. Narrow and Intense Resonances in the Low-Frequency Region of Surface-Enhanced Raman Spectra of Single-Wall Carbon Nanotubes. *Phys. Rev. B* **2010**, *82*, 245402.
34. Liu, K.; Jiang, K. L.; Feng, C.; Chen, Z.; Fan, S. S. A Growth Mark Method for Studying Growth Mechanism of Carbon Nanotube Arrays. *Carbon* **2005**, *43*, 2850–2856.
35. Futaba, D. N.; Hata, K.; Yamada, T.; Mizuno, K.; Yumura, M.; Iijima, S. Kinetics of Water-Assisted Single-Walled Carbon Nanotube Synthesis Revealed by a Time-Evolution Analysis. *Phys. Rev. Lett.* **2005**, *95*, 056104.

36. Einarsson, E.; Murakami, Y.; Kadowaki, M.; Maruyama, S. Growth Dynamics of Vertically Aligned Single-Walled Carbon Nanotubes from "in situ" Measurements. *Carbon* **2008**, *46*, 923–930.
37. Yasuda, S.; Futaba, D. N.; Yumura, M.; Iijima, S.; Hata, K. Diagnostics and Growth Control of Single-Walled Carbon Nanotube Forests Using a Telecentric Optical System for "in situ" Height Monitoring. *Appl. Phys. Lett.* **2008**, *93*, 143115–143117.
38. Amama, P. B.; Pint, C. L.; McJilton, L.; Kim, S. M.; Stach, E. A.; Murray, P. T.; Hauge, R. H.; Maruyama, B. Role of Water in Super Growth of Single-Walled Carbon Nanotube Carpets. *Nano Lett.* **2009**, *9*, 44–49.
39. Zhong, G. F.; Iwasaki, T.; Robertson, J.; Kawarada, H. Growth Kinetics of 0.5 cm Vertically Aligned Single-Walled Carbon Nanotubes. *J. Phys. Chem. B* **2007**, *111*, 1907–1910.
40. Wirth, C. T.; Zhang, C.; Zhong, G. F.; Hofmann, S.; Robertson, J. Diffusion- and Reaction-Limited Growth of Carbon Nanotube Forests. *ACS Nano* **2009**, *3*, 3560–3566.
41. Kim, S. M.; Pint, C. L.; Amama, P. B.; Hauge, R. H.; Maruyama, B.; Stach, E. A. Catalyst and Catalyst Support Morphology Evolution in Single-Walled Carbon Nanotube Supergrowth: Growth Deceleration and Termination. *J. Mater. Res.* **2010**, *25*, 1875–1885.
42. Li, Y.; Kim, W.; Zhang, Y.; Rolandi, M.; Wang, D.; Dai, H. Growth of Single-Walled Carbon Nanotubes from Discrete Catalytic Nanoparticles of Various Sizes. *J. Phys. Chem. B* **2001**, *105*, 11424–11431.
43. Finnie, P.; Li-Pook-Than, A.; Lefebvre, J. Phases of Carbon Nanotube Growth and Population Evolution from in Situ Raman Spectroscopy During Chemical Vapor Deposition. *J. Phys. Chem. C* **2010**, *114*, 11018–11025.